J Solid State Electrochem (2013) 17:2437–2444
DOI 10.1007/s10008-013-2127-y

ORIGINAL PAPER

# The electrochemical properties of Fe- and Ni-cosubstituted $Li_2MnO_3$ via combustion method

**Guo-Biao Liu · Heng Liu · Yan Wang · Yun-Feng Shi · Yun Zhang**

Received: 1 April 2013 / Revised: 3 May 2013 / Accepted: 14 May 2013 / Published online: 24 May 2013


**Abstract** The Co-free $Li_{1.20}Mn_{0.54}Ni_xFe_yO_2$ ($x/y$=0.5, 1.0, 2.0) materials were synthesized by combustion method. The effects of the preparation condition on the structure, morphology, and electrochemical performance were investigated by X-ray diffractometry, scanning electron microscopy, charge–discharge tests, and cyclic voltammetry (CV). The results indicate that the structure and electrochemical characteristics are sensitive to the preparation condition when a large amount of Fe is included. A pure layered $\alpha$-$NaFeO_2$ structure with R-3m space group and the discharge capacities of over 200 mAh $g^{-1}$ were observed in some as-prepared cathode materials. Particularly, the $Li_{1.2}Mn_{0.54}Ni_{0.13}Fe_{0.13}O_2$ prepared by mixing an excess amount of lithium and by firing at 600 °C exhibits a second discharge capacity of 264 mAh $g^{-1}$ in the voltage range of 1.5–4.8 V under current density of 30 mA $g^{-1}$ at 30 °C and discharge capacity of 223 mAh $g^{-1}$ at 2.0–4.8 V. Nevertheless, an unpleasant capacity fading was observed and is primarily ascribed to transformation from a rock-layered structure into a spinel one according to CV testing.

**Keywords** Li-rich solid solution · Fe- and Ni-cosubstituted $Li_2MnO_3$ · Combustion method · Capacity fading

## Introduction

Lithium ion batteries (LIBs) play a predominant role in the storage devices for cellular phones due to their higher energy density, which facilitates smaller batteries with more power. However, new-generation mobile devices, such as the iPad, and electrical vehicles challenge the energy density of LIBs. So far, enhancing the cathode material capacity is believed to be the favorable strategy since the capacity of the present commercialized cathode materials is far lower than that of anode material. For instance, the capacities of $LiCO_2$, $LiMn_2O_4$, $LiFePO_4$, $LiMn_{1/3}Ni_{1/3}Co_{1/3}$, and $LiNi_{0.8}Co_{0.15}Al_{0.05}$ are less than 200 mAh $g^{-1}$. In contrast, the capacity of graphite anode is more than 300 mAh $g^{-1}$. So, the studies of devising a new practical cathode material with higher energy density have been widely conducted.

Li-rich solid solution in the formula of $xLi_2AO_3$ ($A$=Mn,Ti…)·(1−$x$) $LiBO_2$ ($B$=Ni,Co,Mn,…) [1–13] has drawn much attention in recent years because of the inspiring energy density of above 250 Wh $kg^{-1}$, which is attributed to its discharge capacity of over 250 mAh $g^{-1}$ and moderate discharge voltage of above 3.5 V. Among all sorts of the Li-rich solid solutions, Fe- or Fe- and Ni-cosubstituted $Li_2MnO_3$ [14–20] was highlighted on behalf of the cost and environment since Fe is a low-cost, eco-friendly, and resource-wise abundant metal. Especially, the Fe- and Ni-cosubstituted $Li_2MnO_3$ was believed to be more attractive because of its higher average voltage compared with that of Fe-substituted $Li_2MnO_3$. However, the preparation of the Fe- and Ni-cosubstituted $Li_2MnO_3$ with high discharge capacity was supposed to be difficult. In previous literatures, the process [21–23] consisting of three steps (coprecipitation–hydrothermal–calcinations) was believed to be a common method to fabricate Fe-substituted or ($Fe_{1/2}Ni_{1/2}$)-substituted $Li_2MnO_3$ with high discharge capacity over 200 mAh $g^{-1}$ when a considerable amount Fe is taken into account. Recently, a non-hydrothermal method was confirmed to be available for ($Fe_{1/2}Ni_{1/2}$)-substituted $Li_2MnO_3$ [24], which inspired our group to synthesize the Fe- and Ni-cosubstituted $Li_2MnO_3$ by other non-hydrothermal methods. Combustion method is a simple method and was applied to synthesize the Li-rich

G.-B. Liu · H. Liu (✉) · Y.-F. Shi · Y. Zhang
College of Materials Science and Engineering, Sichuan University, Chengdu 610064, People's Republic of China
e-mail: h_liu@scu.edu.cn

Y. Wang
College of Computer Science and Technology, Southwest University for Nationalities, Chengdu 610041, People's Republic of China

layered cathode material without Fe [25]. To our knowledge, the combustion method is still a novel way to fabricate the Fe- and Ni-cosubstituted $Li_2MnO_3$. In this regard, we adopted the combustion method to synthesize this kind of cathode material. Meanwhile, in the latest literature [26], $0.5Li_2MnO_3{\cdot}0.5LiMn_{0.5}Ni_{0.5}O_2$ doped with a slight amount of Fe via non-hydrothermal steps exhibited a discharge capacity of 210 mAh $g^{-1}$, and electrochemical performance was closely related to the amount of doped Fe. So, the effects of the ratio of Ni/Fe on the structure as well as the electrochemical performance were emphasized in our work.

In this work, the formula $Li_{1.20}Mn_{0.54}Ni_{0.13}Fe_{0.13}O_2$ was chosen as the basic one in reference with the literature [24] in which $Li_{1.20}Mn_{0.54}Ni_{0.13}Fe_{0.13}O_2$ material had been fabricated by a non-hydrothermal method. Besides the ratio of Ni/Fe, the amount of lithium mixed during the preparation process and the sintering temperature were taken into consideration as well. What is more, the mechanism for the capacity fading was investigated, since the capacity fading mechanism of Fe-substituted or Fe- and Ni-cosubstituted $Li_2MnO_3$ was uncovered in previous literatures [21–24].

## Experiments

The formulas $Li_{1.2}Mn_{0.54}Ni_{0.087}Fe_{0.173}O_2$ and $Li_{1.2}Mn_{0.54}Ni_{0.173}Fe_{0.087}O_2$ are derived from the variation of Ni/Fe ratio on the basis of $Li_{1.2}Mn_{0.54}Ni_{0.13}Fe_{0.13}O_2$. A firing temperature of 600 °C was used in terms of two factors. Firstly, the calcination temperature of layered cathode material containing Fe, Ni, and Mn is low in the literature [18, 20, 27]. Secondly, $Li_2MnO_3$ can be prepared at 500 °C. In order to understand the impact of the firing temperature on Fe- and Ni-cosubstituted $Li_2MnO_3$ by a combustion method, two samples with the targeted composition $Li_{1.2}Mn_{0.54}Ni_{0.13}Fe_{0.13}O_2$ were prepared at 750 and 900 °C, respectively.

Reagent-grade $Mn(CH_3COO)_2{\cdot}4H_2O$, $Ni(NO_3)_2{\cdot}6H_2O$, $Fe(NO_3)_3{\cdot}9H_2O$, and $LiNO_3$ were used as the starting materials. Firstly, the stoichiometric amounts of the Mn, Ni, Fe, and Li were dissolved in distilled water with the targeted compositions $Li_{1.2}Mn_{0.54}Ni_{0.087}Fe_{0.173}O_2$, $Li_{1.2}Mn_{0.54}Ni_{0.13}Fe_{0.13}O_2$, and $Li_{1.2}Mn_{0.54}Ni_{0.173}Fe_{0.087}O_2$. And then, an appropriate amount of sucrose was added to the solution. The solution was stirred at 95 °C until a viscous gel was attained after evaporation of excess water. A voluminous foamy mass was formed after drying the viscous gel at 150 °C. The voluminous foamy mass spontaneously burned when slowly heated to 400 °C and transformed into a brown precursor which was fired in air at 600 °C for 30 h and cooled directly to room temperature at furnace. These samples were designated as A 600, B 600, and C 600. As far as the evaporation of lithium during the fire was concerned, additional three samples were prepared at 600 °C under condition that an excess 5 % amount of lithium was added in terms of $Li_{1.2}Mn_{0.54}Ni_{0.087}Fe_{0.173}O_2$, $Li_{1.2}Mn_{0.54}Ni_{0.13}Fe_{0.13}O_2$, and $Li_{1.2}Mn_{0.54}Ni_{0.173}Fe_{0.087}O_2$. These samples were designated as A′ 600, B′ 600, and C′ 600. In addition, two samples in terms of $Li_{1.2}Mn_{0.54}Ni_{0.13}Fe_{0.13}O_2$ were prepared at 750 and 900 °C, respectively, in a way of an excess 5 % amount of lithium. These samples were designated as B′ 750 and B′ 900.

Powder X-ray diffraction (XRD, Philips, X'pert TRO MPD) using Cu Kα radiation at 40 kV/25 mA at 0.06° $s^{-1}$ was employed to characterize the crystal phase of samples. Scanning electron microscopy (SEM, JEOL JSM-5900LV) was conducted to check the particle shape and size.

Electrochemical properties of active materials were tested by a CR2032 coin-type lithium half-cell. The positive electrode consisted of 80 wt% active material with 15 wt%

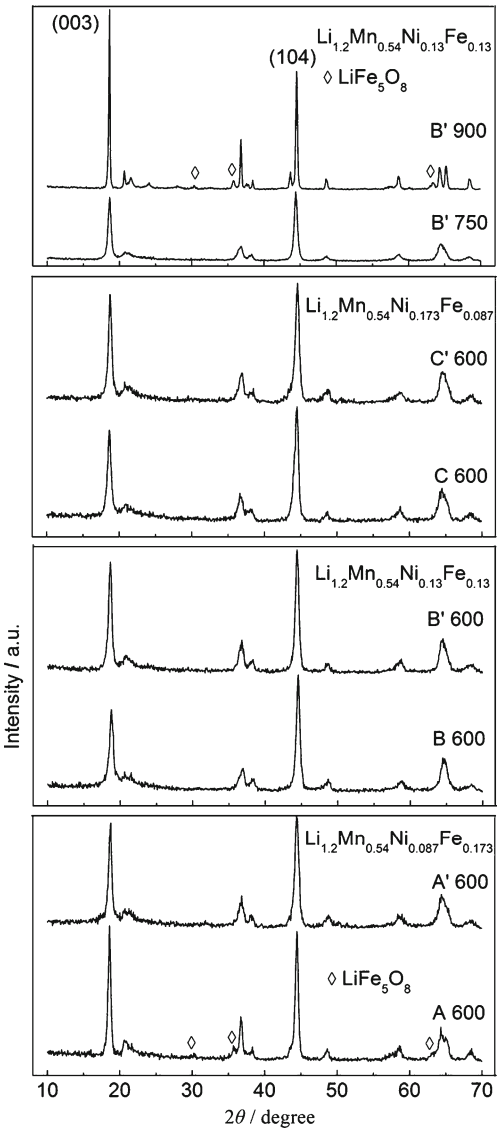


**Fig. 1** XRD patterns for the A 600, A′ 600, B 600, B′ 600, C 600, C′ 600, B′ 750, and B′ 900 compounds *from bottom to top*

acetylene black and 5 wt% carboxymethyl cellulose (an eco-friendly and low-cost binder). Aluminum foil was selected as the current collector of the positive electrode; Li metal was used as a negative electrode. A solution of $LiPF_6$ in ethylene carbonate and dimethyl carbonate ($V_{EC}/V_{DMC}$= 1:1) was selected as an electrolyte. Cell tests started from 30 mA $g^{-1}$ (0.1 C, nominal capacities=300 mAh $g^{-1}$) between 1.5 and 4.8 V of cutoff voltages using a battery test system (Neware BTS-610) at room temperature (about 30 °C). Cyclic voltammograms (CVs) were measured on a LK9805 electrochemical interface at a scanning rate of 0.1 mV $s^{-1}$.

## Results and discussion

### XRD structural characterization

Figure 1 shows the XRD patterns for as-prepared A 600, A′ 600, B 600, B′ 600, C 600, C′ 600, B′ 750, and B′ 900 from bottom to top. An obvious impurity of $LiFe_5O_8$ was checked in the patterns A 600 and B′ 900. Except for three peaks indexed as the $LiFe_5O_8$, the diffraction peaks can be indexed to the monoclinic lattice with space group C2/m in the patterns A 600 and B′ 900. As for other samples, $LiFe_5O_8$ was not detected in those patterns. The peaks can be indexed based on $\alpha$-$NaFeO_2$ structure with R-3m space group in the patterns A′ 600, B 600, B′ 600, C 600, C′ 600, and B′ 750. Additionally, the peaks between 20° and 25° are observed and considered to be caused by the short-range superlattice ordering of Li and Mn in the transition metal layer [1, 21]. It is generally supposed that the cation ordering of the $\alpha$-$NaFeO_2$ structure can be indicated from the $I_{(003)}/I_{(104)}$ peak intensity ratio [25, 27]. The ratios of $I_{(003)}/I_{(104)}$ are shown in Table 1. According to the $I_{(003)}/I_{(104)}$ value, A 600 and B′ 900 ought to exhibit the better electrochemical performance than the other samples do without consideration of the impurity and the particle size. B′ 600, B′ 750, and C′ 600 show roughly the similar $I_{(003)}/I_{(104)}$ value, which means that the B′ 600, B′ 750, and C′ 600 have similar structural properties.

### Morphology

Figure 2 shows the SEM images of as-prepared A 600, A′ 600, B 600, B′ 600, C 600, C′ 600, B′ 750, and B′ 900 from bottom to top. The primary particle size of less than 100 nm was observed in A 600, A′ 600, B 600, B′ 600, C 600. and C ′ 600. A lower extent of agglomeration is observed in B 600 and B′ 600. However, the primary particle size of B′ 750 is slightly greater than that of B′ 600. And then, the primary particle size of B′ 900 increases dramatically and is above 400 nm, which is in accord with the better crystallinity of B′ 900 shown in Fig. 1. In general, a small particle and a lower extent of agglomeration can lead to a higher discharge capacity and a better rate performance [28].

### Electrochemical performance

Figure 3, from bottom to top, shows the initial several charge–discharge curves for A 600, A′ 600, B 600, B′ 600, C 600, C′ 600, B′ 750, and B′ 900 compounds at voltage range between 1.5 and 4.8 V at current density of 30 mA $g^{-1}$. Two plateaus are observed in the initial charge curves at all profiles. One is observed below 4.5 V, and another is around 4.5 V, much the way the initial charge curves of other $Li_2MnO_3{\cdot}LiMO_2$ solid solutions did [1–3]. The former plateau starts from 4.0 V. The redox reaction of $Ni^{4+}/Ni^{2+}$ was supposed to contribute to the former plateau according to earlier reports [24, 27]. The latter plateau starting from the 4.4 V is connected with the extraction of $Li_2O$ from inactive $Li_2MnO_3$. In addition, two plateaus are observed in the second charge curves at profiles for A 600, A′ 600, B 600, B′ 600, C 600, C′ 600, and B′ 750. The former section is between 3.0 and 3.75 V and is attributed to the redox reactions of $Mn^{4+}/Mn^{3+}$ which was observed in some $Li_2MnO_3{\cdot}LiMO_2$ solid solutions [29, 30]. The latter one starts from 3.75 V, and the redox reaction mechanism is unclear.

**Table 1** The preparation condition, structure, and primary particle size for A 600, A′ 600, B 600, B′ 600, C 600, C′ 600, B′ 750, and B′ 900 compounds

| Sample | Target composition | An excess 5 % lithium source | $LiFe_5O_8$ phase | Particle size (nm) | $I_{(003)}/I_{(104)}$ |
|---|---|---|---|---|---|
| A 600 | $Li_{1.2}Mn_{0.54}Ni_{0.087}Fe_{0.173}O_2$ | N/A | Yes | Less than100 | 1.034 |
| B 600 | $Li_{1.2}Mn_{0.54}Ni_{0.137}Fe_{0.13}O_2$ | N/A | N/A | Less than100 | 0.625 |
| C 600 | $Li_{1.2}Mn_{0.54}Ni_{0.173}Fe_{0.087}O_2$ | N/A | N/A | Less than100 | 0.753 |
| A′ 600 | $Li_{1.2}Mn_{0.54}Ni_{0.087}Fe_{0.173}O_2$ | Yes | N/A | Less than100 | 0.813 |
| B′ 600 | $Li_{1.2}Mn_{0.54}Ni_{0.137}Fe_{0.13}O_2$ | Yes | N/A | Less than100 | 0.869 |
| C′ 600 | $Li_{1.2}Mn_{0.54}Ni_{0.173}Fe_{0.087}O_2$ | Yes | N/A | Less than100 | 0.888 |
| B′ 750 | $Li_{1.2}Mn_{0.54}Ni_{0.137}Fe_{0.13}O_2$ | Yes | N/A | Bigger than 100 | 0.889 |
| B′ 900 | $Li_{1.2}Mn_{0.54}Ni_{0.137}Fe_{0.13}O_2$ | Yes | Yes | Bigger than 400 | 1.522 |

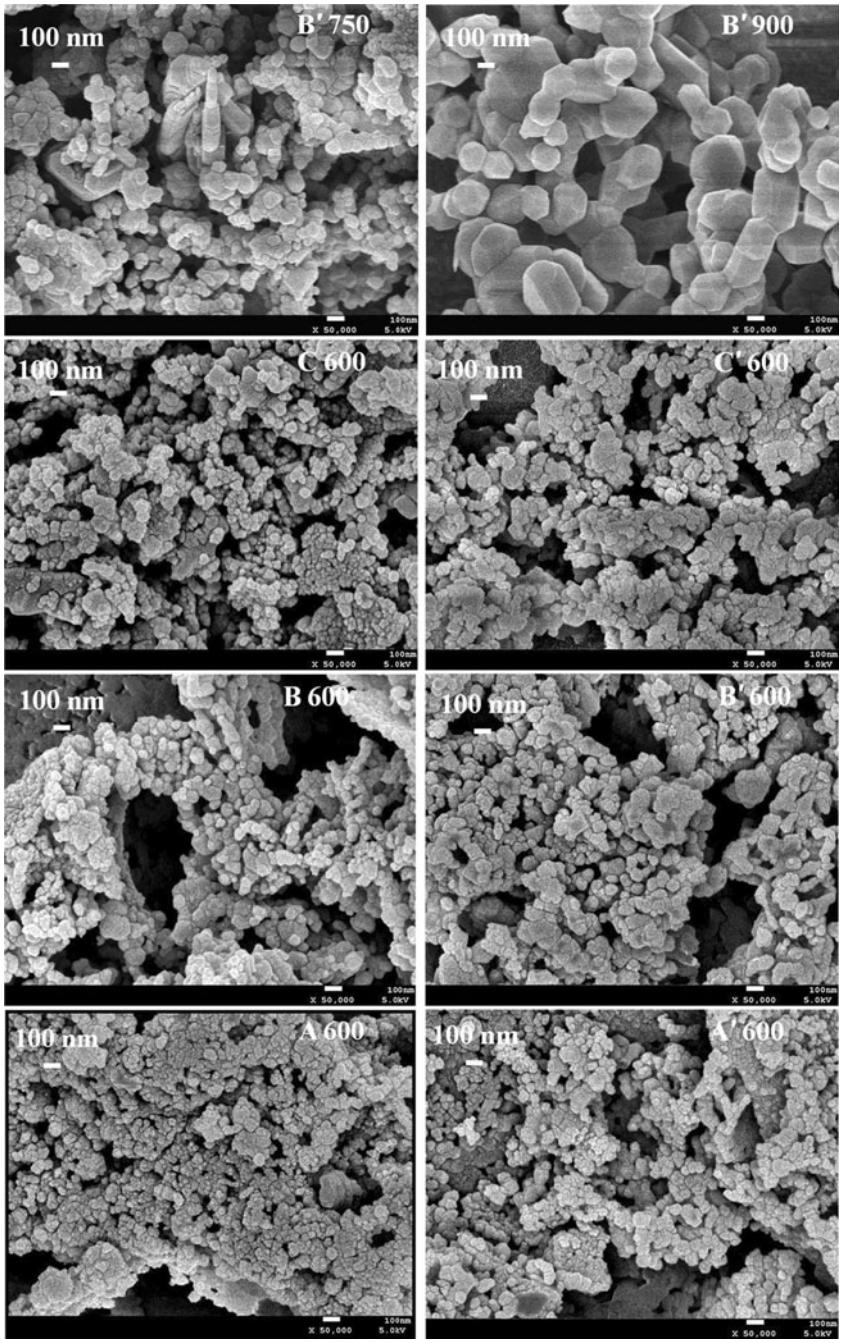


**Fig. 2** SEM images for A 600, A′ 600, B 600, B′ 600, C 600, C ′ 600, B′ 750, and B′ 900 compounds *from bottom to top*

As far as the differences were concerned, an obvious plateau around 1.6 V is observed for A 600, B 600, and C 600. However, the plateau around 1.6 V becomes indistinct for A′ 600, B′ 600, and C′ 600 when an excess amount of lithium is mixed in the process of preparation. The discharge capacities are shown in Table 2. The initial discharge capacities are larger than the second ones for A 600, B 600, and C 600. The initial discharge capacities are smaller than the second ones for A′ 600, B′ 600, and C′ 600. What is more interesting, the second discharge capacities for A′ 600, B′ 600, and C′ 600 are larger than the initial discharge capacities for A 600, B 600, and C 600, respectively, when the cutoff voltage is between 2.0 and 4.8 V. Especially, the second discharge capacity reaches to 223 mAh $g^{-1}$ in the voltage range of 2.0–4.8 V for B′ 600. The larger discharge capacity in the voltage range of 2.0–4.8 V is helpful to practical use since higher average voltage means higher energy density. As the B′ 600 does, the initial discharge capacities for B′ 750 and B′ 900 are smaller than follow-up discharge capacities. Nevertheless, the largest discharge capacity is 193 mAh $g^{-1}$ for B′ 750 when cycling in the voltage range of 1.5–4.8 V, and the largest discharge capacity is 111 mAh $g^{-1}$ for B′ 900. A greater primary particle size is a predominant factor for the unpleasant discharge

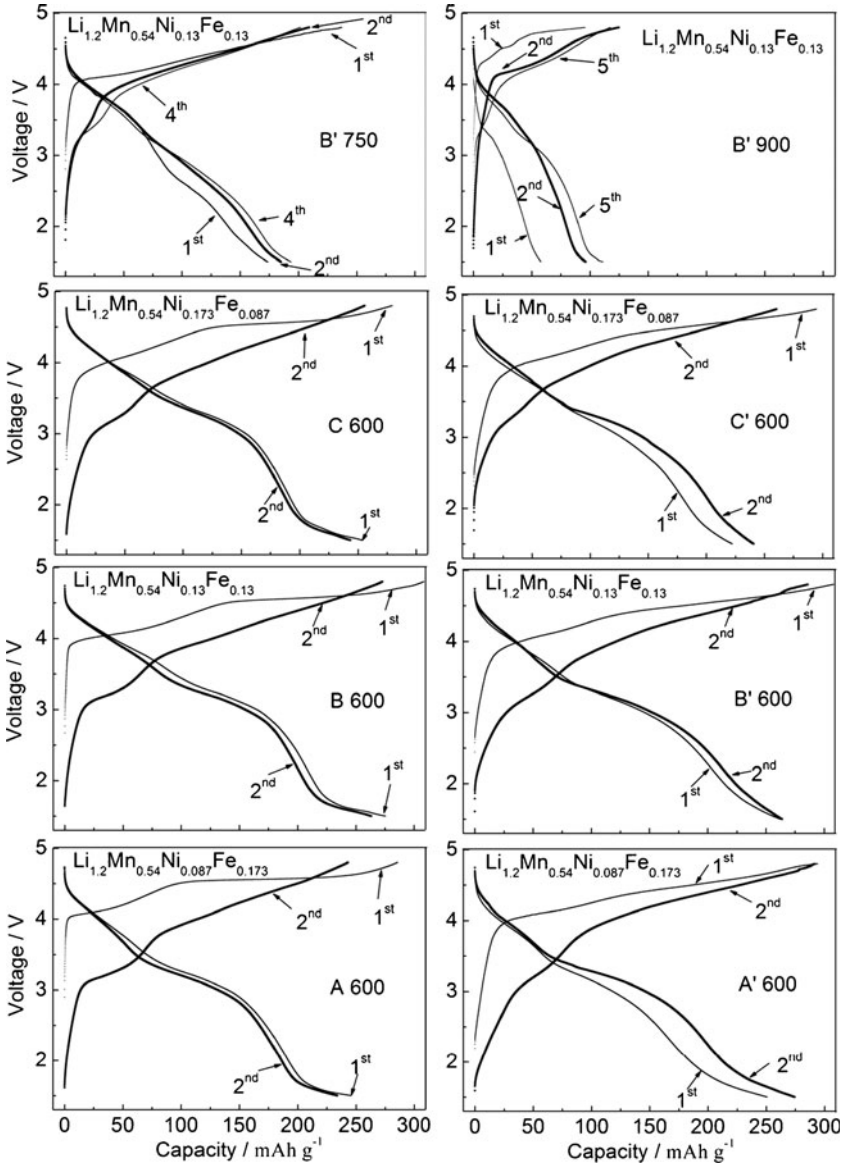


**Fig. 3** Charge–discharge profiles for A 600, A′ 600, B 600, B′ 600, C 600, C′ 600, B′ 750, and B′ 900 compounds between 1.5 and 4.8 V at current density of 30 mA $g^{-1}$. The digits *1st*, *2nd*, *4th*, and *5th* represent the first, second, fourth, and fifth charge–discharge cycle, respectively

capacities for both B′ 750 and B′ 900 in terms of the results from XRD and SEM.

The cyclic voltammograms of B 600 and B′ 600 were conducted in consideration of the better electrochemical

**Table 2** The discharge capacities for the A 600, A′ 600, B 600, B′ 600, C 600, C′ 600, B′ 750, and B′ 900 at 1.5–4.8 and 2.0–4.8 V

| Sample | $Q_{1d,\ 1.5–4.8\ V}$ (mAh $g^{-1}$) | $Q_{2d,\ 1.5–4.8\ V}$ (mAh $g^{-1}$) | $Q_{1d,\ 2.0–4.8\ V}$ (mAh $g^{-1}$) | $Q_{2d,\ 2.0–4.8\ V}$ (mAh $g^{-1}$) |
|---|---|---|---|---|
| A 600 | 245.5 | 234 | 192 | 186 |
| B 600 | 276 | 264 | 213 | 205 |
| C 600 | 254 | 243 | 195 | 191 |
| A′ 600 | 251 | 274 | 185 | 213 |
| B′ 600 | 262 | 264 | 214 | 223 |
| C′ 600 | 223 | 242 | 185 | 206 |
| B′ 750 | 173 | 185 ($Q_{4d}$, 193) | 139 | 157 ($Q_{4d}$, 164) |
| B′ 900 | 57 | 96 ($Q_{5d}$, 111) | 44 | 79 ($Q_{5d}$, 91) |

$Q_{1d}$, initial discharge capacity; $Q_{2d}$, second discharge capacity; $Q_{4d}$, four discharge capacity; $Q_{5d}$, fifth discharge capacity

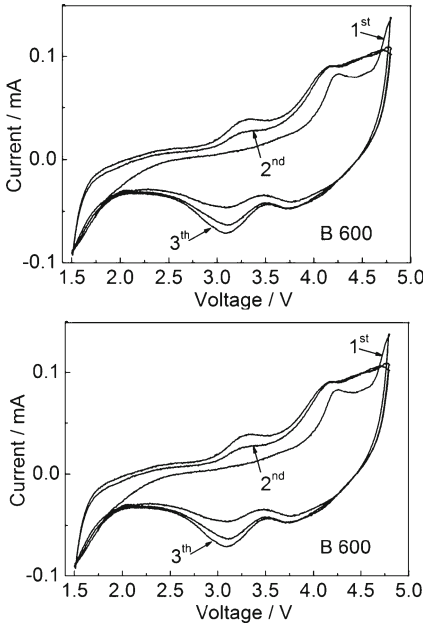


**Fig. 4** The cyclic voltammograms for B 600 and B′ 600

performance for B 600 and B′ 600. The profiles are shown in Fig. 4. An evident oxidation peak is found above 4.5 V in the initial cycle for both samples, which is in line with the presentation of the initial charge plateau around 4.5 V. Simultaneously, an oxidation peak around 4.2 V is observed in the initial cycle for both samples, which is ascribed to the oxidation of $Ni^{2+}$ to $Ni^{4+}$. With exception to the two oxidation peaks, no oxidation peak was detected in the initial cycle. So, it is obvious that the redox reaction of $Mn^{4+}/Mn^{3+}$ is absent in the initial charge process. However, apart from a reduction peak around 3.75 V related to the reduction reaction of $Ni^{4+}$ to $Ni^{2+}$, another reduction peak between 3.0 and 3.5 V was observed in the initial cycle, which is associated with the reduction reaction of $Mn^{4+}/Mn^{3+}$. And then, the $Mn^{4+}$ was activated after the first discharge process. An oxidation peak between 3.0 and 3.5 V is checked in the second cycle. Meanwhile, the reduction peak of $Mn^{4+}/Mn^{3+}$ becomes more

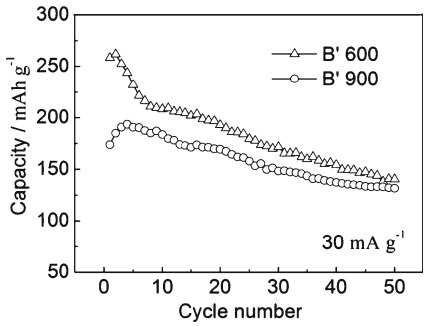


**Fig. 5** Cyclic performance for B′ 600 and B′ 750 between 1.5 and 4.8 V at 30 mA $g^{-1}$

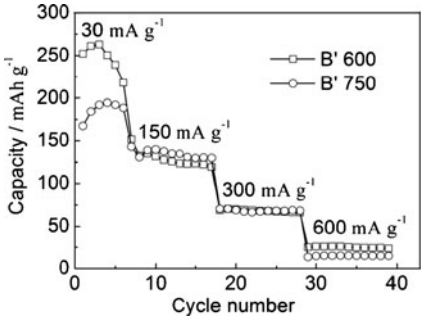


**Fig. 6** Rate capability for B′ 600 and B′ 750 between 1.5 and 4.8 V at 30 °C

evident, which is in agreement with the result of the continuous activated $Mn^{4+}$ in a recent literature [31]. Besides, a reduction peak around 1.5 V is observed in every cycle for both samples. However, the corresponding oxidation peak is absent. According to previous literatures [32, 33], the discharge plateaus of $Fe^{3+}/Fe^{2+}$ is at around 2.6–2.1 V. So, it is hard to associate reduction peak around 1.5 V with the redox reaction of $Fe^{3+}/Fe^{2+}$, though $Fe^{3+}$ was verified as the main form in the Fe- and Ni-cosubstituted $Li_2MnO_3$ in earlier reports [24, 26].

The batteries of B′ 600 and B′ 750 were cycling for 50 cycles on the basis of a higher discharge capacity for B′ 600 in the voltage range of 2.0–4.8 V and a greater amount of iron content. The cyclic properties are shown in Fig. 5. The discharge capacities decline from 262 to 211 mAh $g^{-1}$ for B′ 600 after eight cycles. The capacity retention is 80 % after eight cycles and 73.7 % after 20 cycles, which is the same as that in Fe-substituted $Li_2MnO_3$. The capacity retention was below 78 % after 20 cycles in the cutoff voltage of 1.5–4.8 V in an earlier report [21]. However, the capacity retention is 53 % after 50 cycles. In contrast, the cyclic performance is better for B′ 750. The capacity retention is 96 % after 8 cycles, 87 % after 20 cycles, and 68 % after 50 cycles.

Furthermore, the rate capability were also checked for B′ 600 and B′ 750 under current densities of 150, 300, and

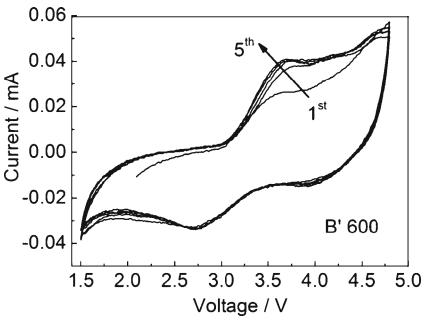


**Fig. 7** The cyclic voltammogram for B′ 600 after 50 charge–discharge cycles

600 mA $g^{-1}$. The rate capability profiles are shown in Fig. 6. As other pristine $Li_2MnO_3{\cdot}LiMO_2$ solid solutions did [34, 35], both B′ 600 and B′ 750 exhibit an awful rate capability. The low electronic conductivity associated with $Mn^{4+}$ [1] or solid electrolyte interface layer [36] and low $Li^+$ diffusion coefficient [37] were supposed as the main factors for the unpleasant rate capability of $Li_2MnO_3{\cdot}LiMO_2$ solid solutions.

In order to disclose the factors for the poor cyclic electrochemical performance, another cyclic voltammogram for B′ 600 was conducted using a battery which had been charged and discharged for 50 cycles. Figure 7 shows cyclic voltammogram curves of the battery of 50 cycles for B′ 600. In contrast to the cyclic voltammogram curves for B′ 600 in Fig. 4, the oxidation peak between 3.0 and 3.5 V is absent. What is more, the reduction peak around 3.2 V moves backward to 2.75 V. According to a previous literature [38], the reduction peak around 2.75 V is originated from a spinel component. So, it is clear that a transformation from a rock-layered phase into a spinel one took place during cycling for B′ 600, which is a factor for the inferior cyclic performance. The successive cyclic voltammogram curves are almost overlapping from cycle 2 to cycle 5, which indicate that the structural transformation predominantly took place at the first 50 cycles.

## Conclusion

The Co-free $Li_{1.20}Mn_{0.54}Ni_xFe_yO_2$ ($x/y$=0.5, 1.0, 2.0) materials were synthesized by a combustion method. The amount of lithium mixed during the preparation process, the ratio of Ni/Fe, as well as the firing temperature played great roles on the structure, morphology, and electrochemical performance. The XRD patterns revealed that $LiFe_5O_8$ was observed in the sample with a larger amount of Fe content when a stoichiometric amount of lithium was mixed in the process of preparation. So as the sample sintered at 900 °C did, regardless of the excess amount of lithium. And then, the materials prepared by mixing an excess amount of lithium and firing at 600 °C possess a layered α-$NaFeO_2$ structure with R-3m space group. However, the electrochemical properties are associated with not only the structure but also the particle size of the as-prepared material. Nevertheless, the Fe- and Ni-cosubstituted $Li_2MnO_3$ exhibits poor cyclic performance. The transformation from a rock-layered phase to a spinel one was confirmed to play a great part on capacity fading. The $Mn^{4+}$ activated during the initial discharge process was supposed as a factor for the high discharge capacity and the structural transformation. How to stabilize $Mn^{4+}$ and tailor the amount of $Mn^{4+}$ are speculated as the instinct solution to poor cyclic capability, on which great efforts will be paid in our further investigation.

## References


1. Thackeray MM, Kang SH, Johnson CS, Vaughey JT, Benedek R, Hackney SA (2007) $Li_2MnO_3$-stabilized $LiMO_2$ (M=Mn, Ni, Co) electrodes for lithium-ion batteries. J Mater Chem 17:3112–3125
2. Johnson CS, Li N, Lefief C, Thackeray MM (2007) Anomalous capacity and cycling stability of $x Li_2MnO_3{\cdot}(1\text{-}x)LiMO_2$ electrodes (M=Mn, Ni, Co) in lithium batteries at 50 °C. Electrochem Commun 9:787–795
3. Johnson CS, Kim JS, Lefief C, Li N, Vaughey JT, Thackeray MM (2004) The significance of the $Li_2MnO_3$ component in 'composite' $Li_2MnO_3{\cdot}(1\text{-}x)LiMn_{0.5}Ni_{0.5}O_2$ electrodes. Electrochem Commun 6:1085–1091
4. Numata K, Sakaki C, Yamanaka S (1997) Synthesis of solid solutions in a system of $LiCoO_2$-$Li_2MnO_3$ for cathode materials of secondary lithium batteries. Chem Lett 26:725–726
5. Robertson AD, Bruce PG (2003) Mechanism of electrochemical activity in $Li_2MnO_3$. Chem Mater 15:1984–1992
6. Liu J, Reeja-Jayan B, Manthiram A (2010) Conductive surface modification with aluminum of high capacity layered $Li[Li_{0.2}Mn_{0.54}Ni_{0.13}Co_{0.13}]O_2$ cathodes. J Phys Chem C 114:9528–9533
7. Zhang LQ, Noguchi H (2003) Novel layered Li-Cr-Ti-O cathode materials related to the $LiCrO_2$-$Li_2TiO_3$ solid solution. J Electrochem Soc 150:A601–A607
8. Zhang LQ, Wang XQ, Noguchi H, Yoshio M, Takada K, Sasakim T (2004) Electrochemical and ex-situ XRD investigations on $(1\text{-}x)LiNiO_2{\cdot}xLi_2TiO_3$($0.05\leq x\leq 0.5$). Electrochim Acta 49:3305–3311
9. Zhang LQ, Takada K, Ohta N, Osada M, Sasakim T (2007) Synthesis and electro-chemistry of new layered $(1\text{-}x)LiVO_2{\cdot}xLi_2TiO_3$($0\leq x\leq 0.6$) electrode materials. J Power Sources 174:1007–1011
10. Shigemura H, Tabuchi M, Sakaebe H, Kobayashi H, Kageyama H (2003) Lithium extraction and insertion behavior of nanocrystalline $Li_2TiO_3{\cdot}LiFeO_2$ solid solution with cubic rock salt structure. J Electrochem Soc 150:A638–A644
11. Kim JS, Johnson CS, Thackray MM (2002) Layered $xLiMO_2{\cdot}(1\text{-}x)Li_2M'O_3$ electrodes for lithium batteries: a study of $0.95LiMn_{0.5}Ni_{0.5}O_2{\cdot}0.05Li_2TiO_3$. Electrochem Commun 4:205–209
12. Moore GJ, Johnson CS, Thackeray MM (2003) The electrochemical behavior of $xLiNiO_2{\cdot}(1\text{-}x)Li_2RuO_3$ and $Li_2Ru_{1-y}Zr_yO_3$ electrodes in lithium cells. J Power Sources 119–121:216–220
13. Kobayashi H, Uebou Y, Tabuchi M, Kageyama H, Yamamoto Y, Matsuoka M, Tamaki J (2003) Structure, physical properties, and charge–discharge characteristics of Fe-doped $Li_2IrO_3$. J Electrochem Soc 50:A1408–A1415
14. Tabuchi M, Shigemura H, Ado K, Kobayashi H, Sakaebe H, Kageyama H, Kanno R (2001) Preparation of lithium manganese oxides containing iron. J Power Sources 97–98:415–419
15. Tabuchi M, Nakashima A, Ado K, Sakaebe H, Kobayashi H, Kageyama H, Tatsumi K, Kobayashi Y, Seki S, Yamanaka A (2005) The effects of preparation condition and dopant on the electrochemical property for Fe-substituted $Li_2MnO_3$. J Power Sources 146:287–293

16. Tabuchi M, Nakashima A, Shigemura H, Ado K, Kobayashi H, Sakaebe H, Kageyama H, Nakamura T, Kohzaki M, Hirano A, Kanno R (2002) Synthesis cation distribution, and electrochemical properties of Fe-substituted $Li_2MnO_3$ as a novel 4V positive electrode material. J Electrochem Soc 149:A509–A524
17. Tabuchi M, Nabeshima Y, Ado K, Shikano M, Kageyama H, Tatsumi K (2007) Material design concept for Fe-substituted $Li_2MnO_3$-based positive electrodes. J Power Sources 174:554–559
18. Park GJ, Lee YS, Kim J, Nahm KS, Sato Y (2007) Synthesis and electrochemical properties of $Li_{1-x}Fe_{0.8}Ni_{0.2}O_2$-$Li_xMnO_2$ (Mn/(Fe+Ni+Mn)=0.8) material. J Power Sources 174:730–734
19. Zheng X, Cao L, Zhu WT, Qiu XP (2007) Synthesis and performance characterization of $Li(Li_{0.15}Ni_{0.21}Fe_{0.21}Mn_{0.45})O_2$ cathode material with good high temperature cyclibility. Acta Chim Sin 65:571–574
20. Li D, Lian F, Qiu WH, Li FS, Chou KC (2012) Fe content effects on electrochemical properties of $0.3Li_2MnO_3{\cdot}0.7LiMn_xNi_xFe_{(1-2x)/2}O_2$ cathode materials. Adv Mater Res 347–353:3518–3521
21. Tabuchi M, Nabeshima Y, Takeuchi T, Tatsumi K, Imaizumi J, Nitta Y (2010) Fe content effects on electrochemical properties of Fe-substituted $Li_2MnO_3$ positive electrode material. J Power Sources 195:834–844
22. Tabuchi M, Nabeshima Y, Ado K, Tatsumi K, Takeuchi T (2011) Manganese-based composite oxide and method for preparing the same. US Patent 8021783
23. Tabuchi M, Nabeshima Y, Takeuchi T, Kageyama H, Tatsumi K, Akimoto J, Shibuya H, Imaizumi J (2011) Synthesis and electrochemical characterization of Fe and Ni substituted $Li_2MnO_3$-an effective means to use Fe for constructing "Co-free" $Li_2MnO_3$ based positive electrode material. J Power Sources 196:3611–3622
24. Liu GB, Liu H, Shi YF (2013) The synthesis and electrochemical properties of $xLi_2MnO_3$-(1-$x$)$MO_2$(M= $Mn_{1/3}Ni_{1/3}Fe_{1/3}$) via co-precipitation method. Electrochim Acta 88:112–116
25. Zheng JM, Wu XB, Yang Y (2011) A comparison of preparation method on the electrochemical performance of cathode material $Li[Li_{0.2}Mn_{0.54}Ni_{0.13}Co_{0.13}]O_2$ for lithium ion battery. Electrochim Acta 56:3071–3078
26. Lian F, Gao M, Qiu WH, Axmann P, Wohlfahrt-Mehrens M (2012) Fe-doping effects on the structural and electrochemical properties of $0.5Li_2MnO_3{\cdot}0.5LiMn_{0.5}Ni_{0.5}O_2$ electrode material. J Appl Electrochem 42:409–417
27. Karthikeyan K, Amaresh S, Lee GW, Aravindan V, Kim H, Kang KS, Kim WS, Lee YS (2012) Electrochemical performance of cobalt free, $Li_{1.2}(Mn_{0.32}Ni_{0.32}Fe_{0.16})O_2$ cathodes for lithium batteries. Electrochim Acta 68:246–253
28. Wu F, Lu HQ, Su YF, Li N, Bao LY, Chen S (2010) Preparation and electrochemical performance of Li-rich layered cathode material, $Li[Ni_{0.2}Li_{0.2}Mn_{0.6}]O_2$, for lithium-ion batteries. J Appl Electrochem 40:783–789
29. Lu ZH, Dahn JR (2002) Understanding the anomalous capacity of $Li/Li[Ni_xLi_{(1/3-2x/3)}Mn_{(2/3-x/3)}]O_2$ cells using in situ X-ray diffraction and electrochemical studies. J Electrochem Soc 149:A815–A822
30. Armstrong AR, Holzapfel M, Novák P, Johnson CS, Kang SH, Thackeray MM, Bruce PG (2006) Demonstrating oxygen loss and associated structural reorganization in the lithium battery cathode $Li[Ni_{0.2}Li_{0.2}Mn_{0.6}]O_2$. J Am Chem Soc 128:8694–8698
31. Yu HJ, Kim H, Wang Y, He P, Asakura D, Nakamura Y, Zhou HS (2012) High-energy 'composite' layered manganese-rich cathode materials via controlling $Li_2MnO_3$ phase activation for lithium-ion batteries. Phys Chem Chem Phys 14:6584–6595
32. Morales J, Santos-Peña J, Trócoli R, Franger S, Rodriguez-Castellón E (2008) Insights into the electrochemical activity of nanosized α-$LiFeO_2$. Electrochim Acta 53:6366–6371
33. Li JG, Li JJ, Luo J, Wang L, He XM (2011) Recent Advances in the $LiFeO_2$-based Materials for Li-ion Batteries. Int J Electrochem Sci 6:1550–1561
34. Martha SK, Nanda J, Veith GM, Dudney NJ (2011) Electrochemical and rate performance study of high-voltage lithium-rich composition: $Li_{1.2}Mn_{0.525}Ni_{0.175}Co_{0.1}O_2$. J Power Sources 199:220–226
35. Song BH, Lai MO, Lu L (2012) Influence of Ru substitution on Li-rich $0.55Li_2MnO_3{\cdot}0.45LiNi_{1/3}Co_{1/3}Mn_{1/3}O_2$ cathode for Li-ion batteries. Electrochim Acta 80:187–195
36. Wang QY, Liu J, Vadivel Murugan A, Manthiram A (2009) High capacity double-layer surface modified $Li[Li_{0.2}Mn_{0.54}Ni_{0.13}Co_{0.13}]O_2$ cathode with improved rate capability. J Mater Chem 19:4965–4972
37. Li Z, Du F, Bie XF, Zhang D, Cai YM, Cui XR, Wang CZ, Chen G, Wei YJ (2010) Electrochemical kinetics of the Li $[Li_{0.23}Co_{0.3}Mn_{0.47}]O_2$ cathode material studied by GITT and EIS. J Phys Chem C 114:22751–22757
38. Kim DH, Kang SH, Balasubramanian M, Johnson CS (2010) High-energy and high-power Li-rich nickel manganese oxide electrode materials. Electrochem Commun 12:1618–1621